

Supplementary Information for Cycling State that Can Lead to Glassy Dynamics in Intracellular Transport

Monika Scholz,^{1,2} Stanislav Burov,³ Kimberly L. Weirich,^{1,2} Björn J. Scholz,^{4,5,6}

S. M. Ali Tabei,⁷ Margaret L. Gardel,^{1,2,6} and Aaron R. Dinner^{1,2,8,*}

¹*James Franck Institute, the University of Chicago, Chicago, IL 60637*

²*Institute for Biophysical Dynamics, the University of Chicago, Chicago, IL 60637*

³*Department of Physics, Bar-Ilan University, Ramat-Gan, 5290002 Israel*

⁴*Enrico Fermi Institute, the University of Chicago, Chicago, IL 60637*

⁵*Kavli Institute for Cosmological Physics, the University of Chicago, Chicago, IL 60637*

⁶*Department of Physics, the University of Chicago, Chicago, IL 60637*

⁷*Physics Department, University of Northern Iowa Cedar Falls, Iowa 50614*

⁸*Department of Chemistry, the University of Chicago, Chicago, IL 60637*

I. ALTERNATIVE MODELS

Here we illustrate that the results are robust for alternative formulations of the model. First, we tested a model with a one-step binding process. In this scheme, the probability p of a motor at distance d_i to be attached and active is

$$p(d_i) = \frac{\exp[-(3d_i/2s)^2]}{\exp[-E_0] + \sum_i \exp[-(3d_i/2s)^2]}.$$

Here, E_0 is the maximum attractive energy that can be achieved by binding, relative to the unbound state. Fig. S1 compares the MSD results for this scheme and that in the main text.

Second, we explored alternative ways of moving the motors in response to the forces. We proposed the projection rule in the main text to ensure that motors walk parallel to tracks, as observed in many experiments. When this requirement is relaxed, the velocity at each time step can be written as $\vec{v} = \sum_i k_i \vec{e}_i$, where k_i is the number of binding sites attached to filament i and \vec{e}_i is the unit vector in the direction of the filament. The position update then becomes $\vec{x}(t+dt) = \vec{v}dt$. We recover aging and similar values for the MSD scaling exponent under this relaxed assumption (Fig. S2).

II. EFFECT OF NONERGODICITY ON LAG-TIME EXPONENTS

The scaling of the MSD with lag time is dependent on the duration of the recording (measurement time) T . Since experimental data are often limited to short trajectories, we show the resulting time-averaged MSD exponents for shorter simulation times in Fig. S3.

Additionally, we show the trajectories for different binding radii and temporal coarse-grainings Δ (Fig. S4). When Δ is larger than the average trapping time in a vortex, the time-averaged MSD is diffusive.

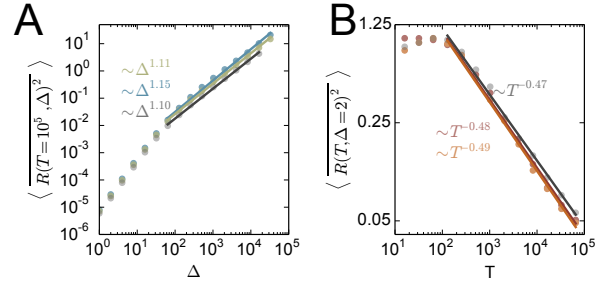


FIG. S1. Mean-squared displacement for a Boltzmann binding scheme (colored curves), compared with results for the two-step attachment scheme in the main text (gray). (A) Time-averaged mean square displacement (MSD) for $E_0 = 0.1$ (green) and $E_0 = 0.5$ (blue). (B) The MSD as a function of measurement time for $E_0 = 0.1$ (orange) and $E_0 = 0.5$ (red). Other parameters are the same as those in the main text (Table 1).

III. EXPERIMENTAL DETAILS

Networks of bundled actin were polymerized in a thin layer at a surface of a flowcell. A supported lipid bilayer passivated the surface. The supported bilayer was formed by incubating a UV-ozone cleaned borosilicate coverslip (Fisherbrand) with 1 mM vesicle suspension. Vesicles were prepared by the standard method of extrusion (200 nm and 50 nm pore membranes, Liposofast extruder, Avestin) from dried films of phospholipid (1,2-dioleoyl-sn-glycero-3-phosphocholine, Avanti Polar Lipids) suspended in buffer (140 mM NaCl, 8.5 mM Na_2HPO_4 , 1.5 mM NaH_2PO_4 , pH 7.5). After a complete bilayer formed, excess vesicle suspension was exchanged with actin polymerization buffer (10 mM imidazole, 50 mM KCl, 0.2 mM EGTA pH 7.5, 300 μM ATP). Monomeric actin (rabbit skeletal muscle purified from acetone powder, Pel-freeze; 2.0 μM unlabeled and 0.64 μM labeled with the fluorophore tetramethylrhodamine-6-maleimide, Life Technologies) was added to initiate the polymerization of long, entangled actin. Depletion agent (0.3 wt %, 15 centipoise methylcellulose, Sigma) crowded actin to the

* To whom correspondence may be addressed: dinner@uchicago.edu

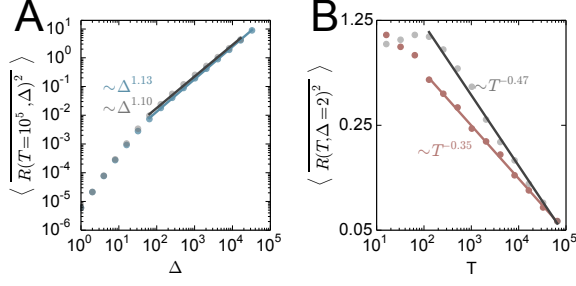


FIG. S2. Mean-squared displacement for the model with a net velocity (red and blue). Results for the two-step attachment scheme in the main text are shown in gray. The parameters used are the same as those in the main text (Table 1).

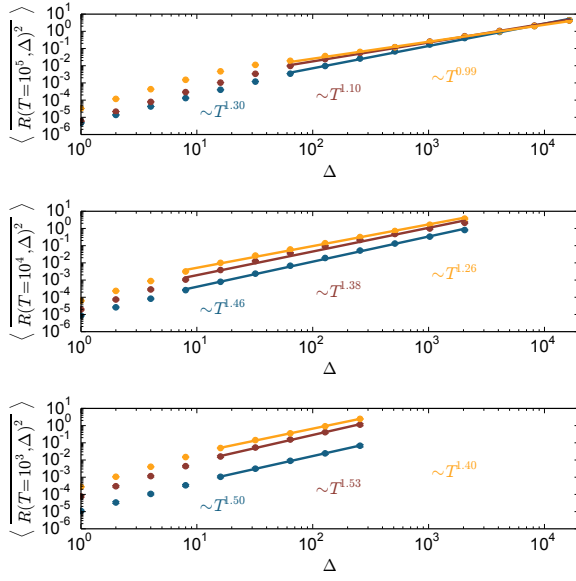


FIG. S3. MSD as a function of lag time for binding radii $s = 0.001$ (blue), 0.01 (red), 0.1 (yellow), and duration of simulation $T = 10^5$, 10^4 and 10^3 (from top to bottom). The parameters used are the same as those in the main text (Table 1).

surface. We used an oxygen scavenging system ($50 \mu\text{M}$ glucose, $0.5 \text{ vol } \%$ β -mercaptoethanol, glucose oxidase, and catalase) to reduce photobleaching. After 30 min of polymerization, fimbrin ($0.53 \mu\text{M}$, pombe) was added to crosslink the actin filaments into a network of bundles. Thick filaments of myosin II were polymerized in a similar manner by adding monomeric myosin II (20 nM , chicken skeletal muscle, fluorescently labeled with Alexa 647, Life Technologies) to a separate, actin-free solution. After 10 min of polymerization, myosin in ATP ($\sim 2\%$ of total sample volume) was gently mixed with the solution above the actin network, such that the final concentrations were 3.8 pM myosin and 2.3 mM ATP. Actin and

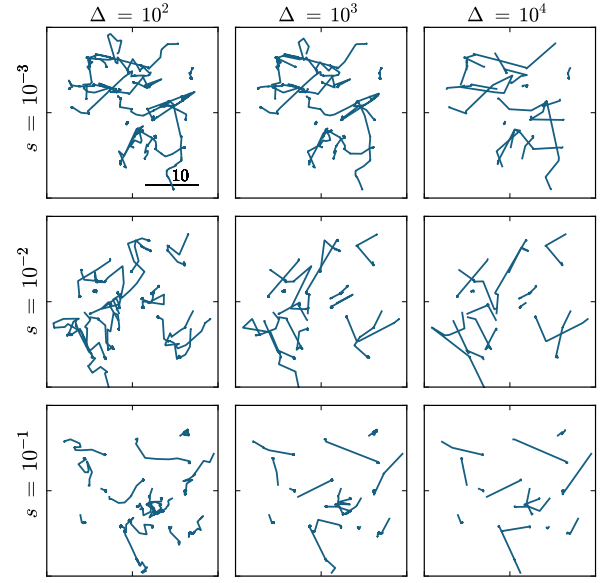


FIG. S4. Example trajectories for binding radii $s = 0.001$, 0.01 , and 0.1 . The trajectories are coarse-grained by only showing points that are temporally separated by Δ . The parameters used are the same as those in the main text (Table 1).

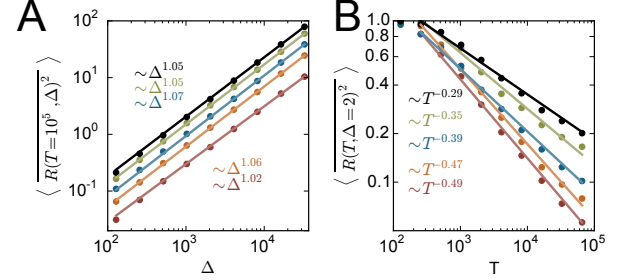


FIG. S5. Mean-squared displacement for different filament network densities. (A) MSD as a function of lag time for network density (number of filaments per unit area) $d = 1$ (red), $d = 2$ (orange), $d = 3$ (blue), and $d = 4$ (green) and $d = 5$ (black). (B) The MSD as a function of measurement time for the same densities as in (A). Other parameters are the same as those in the main text (Table 1).

myosin were imaged with a inverted microscope (Nikon Eclipse Ti-PFS) equipped with a spinning disk confocal head (CSUX, Yokogawa), 561 nm and 647 nm laser lines, $60\times/1.49 \text{ NA}$ oil immersion objective (Zeiss), and a CCD camera (Coolsnap HQ2, Photometrics). Images, collected at 1.5 s intervals, began $\sim 10 \text{ min}$ after myosin was added to the sample.

Single-particle trajectories were obtained using the Python-based implementation of the Crocker-Grier algorithm Trackpy. The settings are given in Tab. I. The

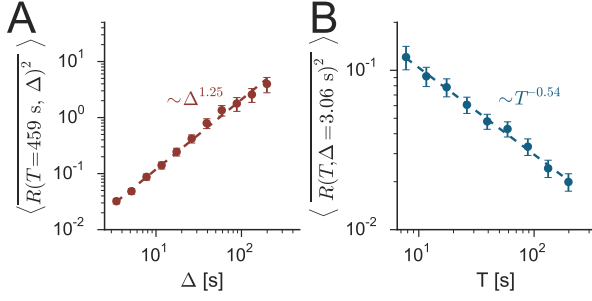


FIG. S6. Mean-squared displacement for myosin II motors. (A) MSD as a function of lag time. (B) The MSD as a function of measurement time.

Parameter	Value
mask diameter	19
minimum mass	650000
noise size	3
search range	15
memory	1

TABLE I. Particle tracking parameters for Trackpy.

particle identification parameters were chosen such that all visible features were detected and the mask size was chosen large enough to obtain subpixel resolution (The histogram of the decimal values of the identified particles showed a flat distribution, indicating no bias within a pixel.). The linking values were set by looking at a previously manually tracked data set and using the largest displacement of that dataset as search range. All other parameters were set to the default values. We quantify the static tracking error for brighter and dimmer objects (implemented in Trackpy). The Fig. S8 shows the ensemble averaged tracking error as a function of time. There is no overall trend in the accuracy over the time of tracking in high (red) or low (blue) brightness fluorescent objects, and there is no statistical difference in the mean tracking error between the two populations (mean and standard deviation shown, unequal variances *t*-test *p*-value=0.0459)

IV. ANALYSIS OF TRAPPED STATES

Here, we consider the possibility that detachment could give rise to the power-law dwell times evidenced by the decay of the MSD with the measurement time. If detachment were responsible for the anomalous dynamics, the particles should undergo simple diffusion when apparently trapped. To test for this possibility, we divided the trajectories between trapped and non-trapped periods and then analyzed their dynamics as follows.

To define the trapped portions of single-particle trajectories, we calculated the average position of each particle

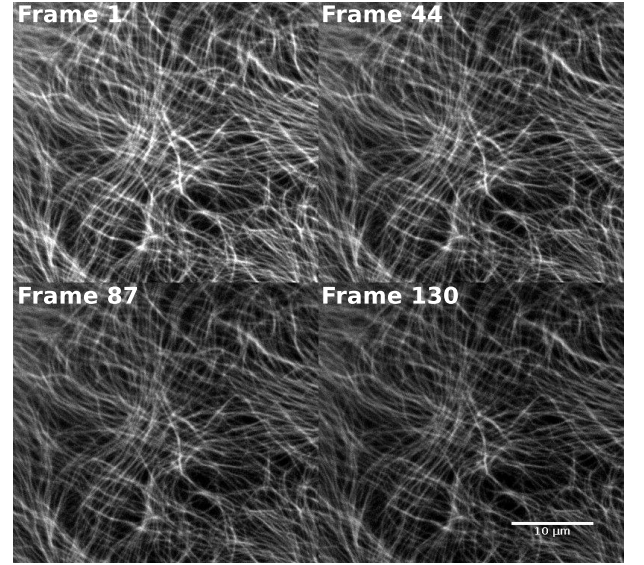


FIG. S7. Fluorescently labelled actin network. The images show snapshots of the actin network while myosin II motors are moving on it (not shown). While the frames show some photobleaching over the course of the experiments, the network does not remodel.

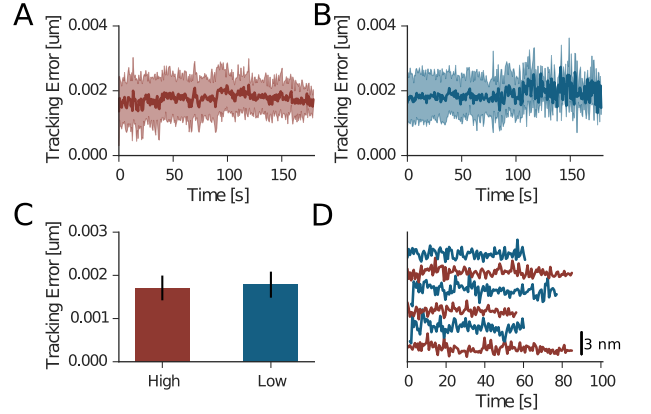


FIG. S8. (A, B) Tracking accuracy for trajectories with high (red) or low (blue) fluorescence. The shaded area denotes the standard deviation. (C) Mean tracking accuracy for high and low fluorescence trajectories. Lines indicate standard deviations. (D) Tracking error for randomly selected trajectories over time.

(motor) every 40 frames. We then compared the instantaneous positions with the averaged ones. If a point in a trajectory deviated by less than 2.0 pixel widths (182 nm) from the corresponding average position, we count that frame as trapped. The results are shown in Figure S9. Representative trapped trajectory segments are shown in red in the context of the non-trapped segments and the filament network (Figure S9A) and in a magnified view (Figure S9B).

To test for simple diffusion with a time resolution of

a few frames, we employ the relative angle distribution introduced by Burov *et al.* [1]. The relative angle is defined by

$$\cos \theta(t; \Delta) = \frac{\vec{v}(t; \Delta) \cdot \vec{v}(t + \Delta; \Delta)}{|\vec{v}(t; \Delta)| |\vec{v}(t + \Delta; \Delta)|}. \quad (1)$$

$\vec{v}(t; \Delta) = \vec{x}(t + \Delta) - \vec{x}(t)$, $\vec{x}(t)$ is the position at time t , and Δ is the lag time as in the present paper. Here we use $\Delta = 1$ frame. We build a histogram of these values for the trapped (red) trajectory segments and normalize such that it integrates to one.

The relative angle distribution for the trapped trajectory segments is shown in Figure S9C. If the motion were simple diffusion, the distribution would be flat, because there would be no directional correlation between steps of the random walk. Instead, we see that it is peaked at $\Theta = \pi$, which indicates that the particles are making reversals. The only way that this could happen from detachment would be if the particles were caged when off the filaments. However, this cannot be the case, as the prevalent switching between trapped and non-trapped states shows that the majority of the particles are unimpeded by obstacles. The only possibility consistent with Figure S9C is that the particles are switching direction while on the filaments, owing to the motor dynamics—this is the cycling mechanism that we propose.

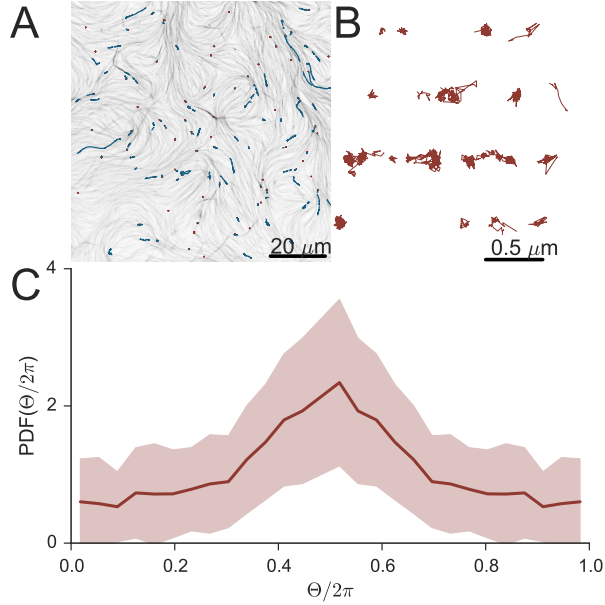


FIG. S9. The dynamics in apparent trapped states are not simple diffusion. (A) Representative single-particle trajectories colored by whether they are assigned to be trapped (red) or not (blue) according to the criteria in the accompanying text. The actin network is shown in gray in the background. (B) Magnified view of selected trapped trajectory segments. (C) Relative angle distribution of trapped trajectory segments for $\Delta = 1$ frame. Shaded area indicates standard deviation.

-
- [1] Stanislav Burov, SM Ali Tabei, Toan Huynh, Michael P Murrell, Louis H Philipson, Stuart A Rice, Margaret L Gardel, Norbert F Scherer, and Aaron R Dinner, “Distribution of directional change as a signature of complex dynamics,” *Proc. Natl. Acad. Sci. USA* **110**, 19689–19694 (2013).